Angewandte International Edition Chemie

… enables the oxidation of a C–H group to an alcohol and finally to a ketone in the presence of manganese(II). This surprise transformation is reminiscent of the story of "The Ugly Duckling", written by Hans Christian Andersen (1805–1875). The picture shows the intermediate homoleptic Mn^{III} complex coordinated by two newly formed alkoxide groups, which is analyzed by C. J. McKenzie et al. in their Communication on page 545 ff. Painting: Johannes Larsen (1867–1961).

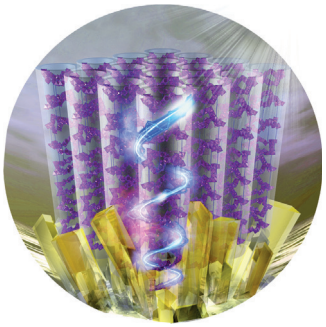

Nanotube Arrays

A metal-halide-based crystalline nanotube array is constructed from a giant $[Pb^{II}_{18}I_{54}(I_2)_9]$ wheel cluster by G. Xu, G.-C. Guo, and co-workers in their Communication on page 514 ff.

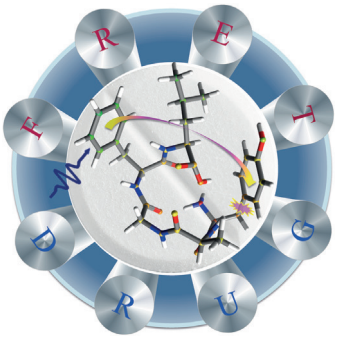

Peptide Structure

The distance between the two aromatic rings of the opioid peptides enkephalins is estimated by V. Kopysov and O. V. Boyarkin by the use of resonance energy transfer as described in their Communication on page 689 ff.

Hydrogenases

In their Communication on page 724 ff., S. Ogo and co-workers develop a dioxygen-tolerant hydrogenase mimic that also catalyzes O_2 reduction and is based on a NiFe core with a strongly electron-donating Cp* ligand.

How to contact us:

Editorial Office:
E-mail: angewandte@wiley-vch.de
Fax: (+49) 62 01–606-331
Telephone: (+49) 62 01–606-315

Reprints, E-Prints, Posters, Calendars:
Carmen Leitner
E-mail: chem-reprints@wiley-vch.de
Fax: (+49) 62 01–606-331
Telephone: (+49) 62 01–606-327

Copyright Permission:
Bettina Loycke
E-mail: rights-and-licences@wiley-vch.de
Fax: (+49) 62 01–606-332
Telephone: (+49) 62 01–606-280

Online Open:
Margitta Schmitt
E-mail: angewandte@wiley-vch.de
Fax: (+49) 62 01–606-331
Telephone: (+49) 62 01–606-315

Subscriptions:
www.wileycustomerhelp.com
Fax: (+49) 62 01–606-184
Telephone: 0800 1800536 (Germany only)
+44(0) 1865476721 (all other countries)

Advertising:
Marion Schulz
E-mail: mschulz@wiley-vch.de
Fax: (+49) 62 01–606-550
Telephone: (+49) 62 01–606-565

Courier Services:
Boschstrasse 12, 69469 Weinheim

Regular Mail:
Postfach 101161, 69451 Weinheim

Angewandte Chemie International Edition is a journal of the Gesellschaft Deutscher Chemiker (GDCh), the largest chemistry-related scientific society in continental Europe. Information on the various activities and services of the GDCh, for example, cheaper subscription to *Angewandte Chemie International Edition*, as well as applications for membership can be found at **www.gdch.de** or can be requested from GDCh, Postfach 900440, D-60444 Frankfurt am Main, Germany.

GDCh
Gesellschaft Deutscher Chemiker

Service

Spotlight on Angewandte's Sister Journals 476 – 479

Author Profile

Hideki Yorimitsu 480

"If I were not a scientist, I would be a diplomat. The most exciting thing about research is one can try many crazy ideas, and some of them turn out to be not so crazy …"
This and more about Hideki Yorimitsu can be found on page 480.

News

Nagoya Gold Medal: S. L. Schreiber 481

Nagoya Silver Medal: Z. Hou 481

Kyoto Prize (Advanced Technology): K. Kunitake 481

François Gault Lectureship: J. Sauer 481

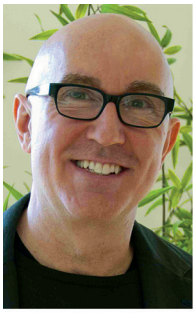
S. L. Schreiber


Z. Hou

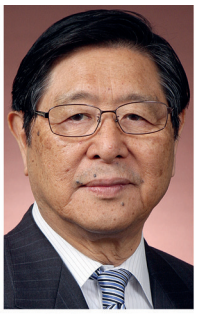
T. Kunitake


J. Sauer

Highlights

Mononuclear Bismuth Compounds

C. Lichtenberg* ——— 484 – 486

Well-Defined, Mononuclear Bi^{I} and Bi^{II} Compounds: Towards Transition-Metal-Like Behavior

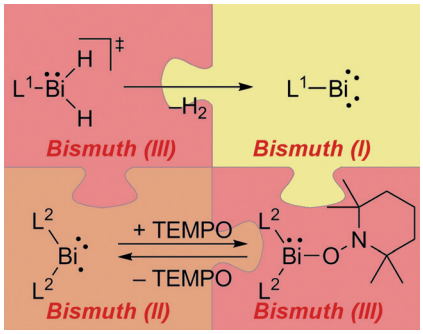

Mononuclear Bi^{I} and Bi^{II} compounds remained elusive for a long time, but recently, the isolation and characterization of such species were reported. They can be handled in solution at ambient temperature and show exceptional properties, which are expected to reveal new reactivity patterns, enabling the development of new catalytic processes. TEMPO = 2,2,6,6-tetramethyl-1-piperidinyl *N*-oxide.

Essays

Drug Design

C. W. Murray, D. C. Rees* ——— 488 – 492

Opportunity Knocks: Organic Chemistry for Fragment-Based Drug Discovery (FBDD)

What's a good fragment? Fragment-based drug discovery is well-established within many pharmaceutical, biotech, and academic institutions for generating new drugs. In this Essay, the opportunities and challenges for organic chemists to design and synthesize new fragments are described.

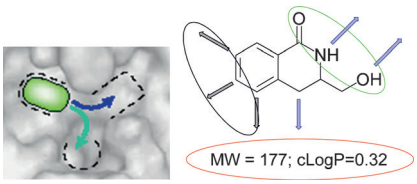

Minireviews

Synthetic Methods

M. Oestreich* ——— 494 – 499

Transfer Hydrosilylation

Fair trade: Transfer hydrosilylation is a technique that, unlike the conceptually related transfer hydrogenation, had not been considered for nearly a century. The recently developed radical and ionic transition-metal-free variants rely on aromatization of a cyclohexa-1,4-diene during release of a silicon radical and cation, respectively. Subsequent reaction with typical unsaturated substrates (e.g. alkenes) terminates the transfer process (see scheme).

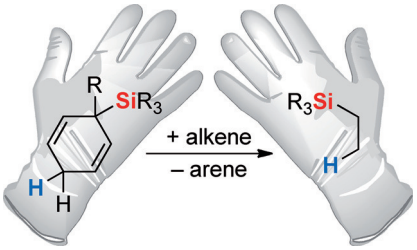

For the USA and Canada:
ANGEWANDTE CHEMIE International Edition (ISSN 1433-7851) is published weekly by Wiley-VCH, PO Box 101161, 69451 Weinheim, Germany. US mailing agent: SPP, PO Box 437, Emigsville, PA 17318. Periodicals postage paid at Emigsville, PA. US POSTMASTER: send address changes to *Angewandte Chemie*, John Wiley & Sons Inc., C/O The Sheridan Press, PO Box 465, Hanover, PA 17331. Annual subscription price for institutions: US$ 16.862/14.051 (valid for print and electronic / print or electronic delivery); for individuals who are personal members of a national chemical society prices are available on request. Postage and handling charges included. All prices are subject to local VAT/sales tax.

Reviews

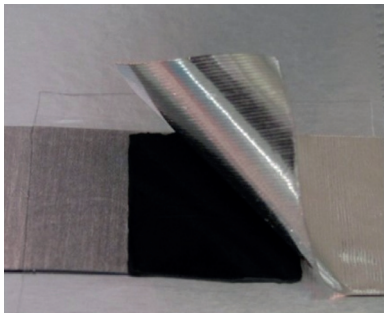

Safety net: Polymer electrolytes are a safe alternative to conventional liquid electrolytes in lithium batteries. Their main drawback is low ionic conductivity at room temperature. The most promising solution for this issue is incorporation of ionic liquids, which enhance the performance without decline in safety. This Review elucidates the interactions in these ternary polymer electrolytes and their performance in lithium-metal polymer batteries.

Lithium Batteries

I. Osada, H. de Vries, B. Scrosati,* S. Passerini* ——— **500 – 513**

Ionic-Liquid-Based Polymer Electrolytes for Battery Applications

Communications

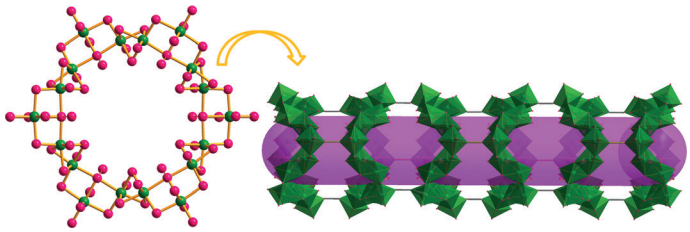

Lead the way to the tube: The first example of a metal-halide-based crystalline nanotube array is constructed from an unprecedented giant $[Pb^{II}_{18}I_{54}(I_2)_9]$ wheel cluster (see picture, Pb green, I pink). It has typical semiconductive properties and highly anisotropic conductivity.

Inorganic Nanotubes

G.-E Wang, G. Xu,* B.-W. Liu, M.-S. Wang, M.-S. Yao, G.-C. Guo* ——— **514 – 518**

Semiconductive Nanotube Array Constructed from Giant $[Pb^{II}_{18}I_{54}(I_2)_9]$ Wheel Clusters

Frontispiece

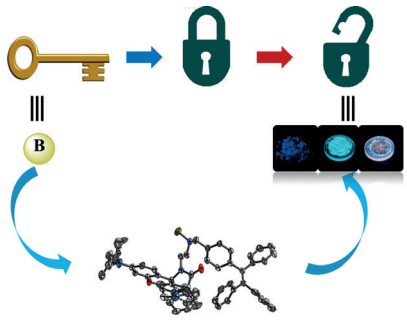

Tricolor switch: A single crystal of M-4-B was obtained by attaching the boron of BH_3 to the amine linker between a tetraphenylethylene unit and rhodamine B. M-4-B showed a novel sequential tricolor switching from deep-blue to bluish-green and to a reddish color upon grinding. The boron atom played a key role in obtaining the single crystal (see picture: O red, N blue, B yellow).

Mechanochromic Fluorescence

Z. Y. Ma, Z. J. Wang, X. Meng, Z. M. Ma, Z. J. Xu, Y. G. Ma,* X. R. Jia* ——— **519 – 522**

A Mechanochromic Single Crystal: Turning Two Color Changes into a Tricolored Switch

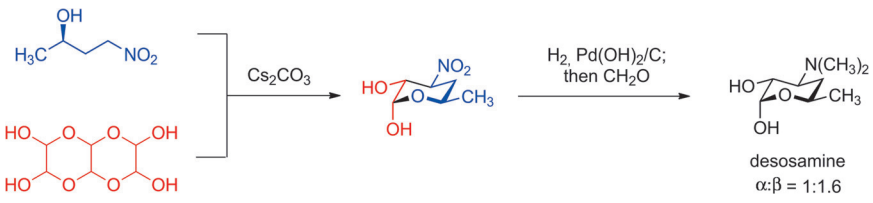

Concise and practical: D-Desosamine is synthesized in 4 steps (27.5% yield) from methyl vinyl ketone and sodium nitrite. The key step in this chromatography-free synthesis is the Cs_2CO_3-mediated coupling of (*R*)-4-nitro-2-butanol and glyoxal, which affords in crystalline form 3-nitro-3,4,6-trideoxy-α-D-glucose, a nitro sugar stereochemically homologous to D-desosamine.

Amino Sugar Synthesis

Z. Zhang, T. Fukuzaki, A. G. Myers* ——— **523 – 527**

Synthesis of D-Desosamine and Analogs by Rapid Assembly of 3-Amino Sugars

Cancer Imaging

M. Rashidian, L. Wang, J. G. Edens, J. T. Jacobsen, I. Hossain, Q. Wang, G. D. Victora, N. Vasdev,* H. Ploegh,* S. H. Liang* ——— 528 – 533

Enzyme-Mediated Modification of Single-Domain Antibodies for Imaging Modalities with Different Characteristics

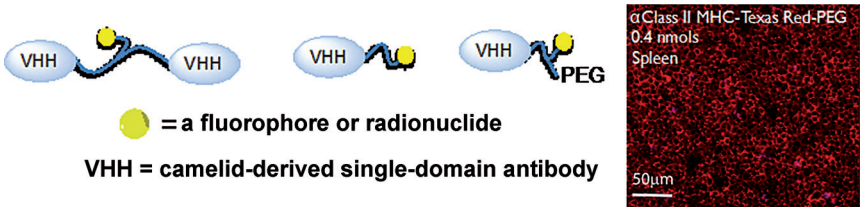

Improve your image! Dual labeling of antibody fragments with a fluorophore or ^{18}F isotope for multimodal imaging and with a PEG moiety or a second antibody fragment to improve circulatory half-life or avidity led to constructs that recognized Class II MHC products (see picture) and CD11b with high specificity. PET imaging with the constructs enabled the detection of tumors as small as a few millimeters in size.

Homogeneous Catalysis

Y.-A. Yuan, D.-F. Lu, Y.-R. Chen, H. Xu* ——— 534 – 538

Iron-Catalyzed Direct Diazidation for a Broad Range of Olefins

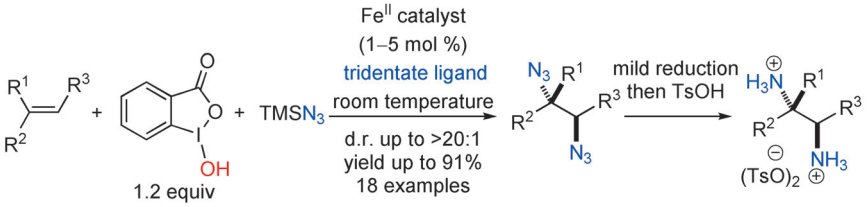

With iron hand: The title reaction proceeds at room temperature and tolerates a broad range of both unfunctionalized and highly functionalized olefins. It also provides a convenient synthetic approach to a variety of nitrogen-containing building blocks. Preliminary mechanistic studies suggest both Lewis acid activation and iron-enabled redox catalysis are crucial for the selective azido-group transfer.

Hydrogen Bonding

A. K. Turek, D. J. Hardee, A. M. Ullman, D. G. Nocera,* E. N. Jacobsen* ——— 539 – 544

Activation of Electron-Deficient Quinones through Hydrogen-Bond-Donor-Coupled Electron Transfer

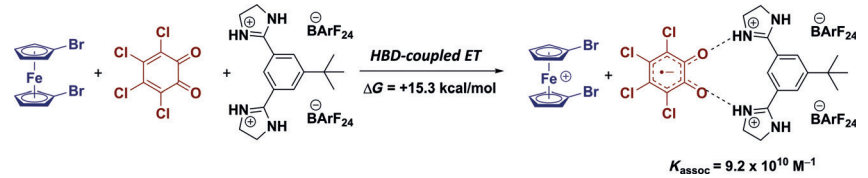

Electron transfer made easier: Electron transfer (ET) to electron-deficient quinones is facilitated through the use of dicationic hydrogen-bond donors (HBDs) as the large thermodynamic barrier is surmounted through strong association between the HBD and the reduced quinone. The use of an HBD also accelerates the rate of the electron-transfer event by up to twelve orders of magnitude.

C–H Oxidation

C. Deville, S. K. Padamati, J. Sundberg, V. McKee, W. R. Browne, C. J. McKenzie* ——— 545 – 549

O_2 Activation and Double C–H Oxidation by a Mononuclear Manganese(II) Complex

Front Cover

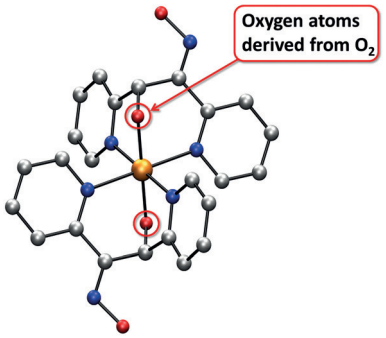

A mononuclear manganese(II) complex of a new oxime-dipyridyl ligand activates O_2. Catalytic methylene C–H oxidation of the ligand then yields an alkoxide and finally a ketone in a stepwise process. Bis-(manganese) complexes of the ligand in its various stages of oxidation were structurally characterized.

Membrane proteins: Gas-phase dissociation of membrane proteins in nanodisc lipoprotein complexes by collisional activation yielded membrane proteins with many lipids bound in distinct shells. High-resolution orbitrap mass spectrometry provided unprecedented resolution of the dissociation products.

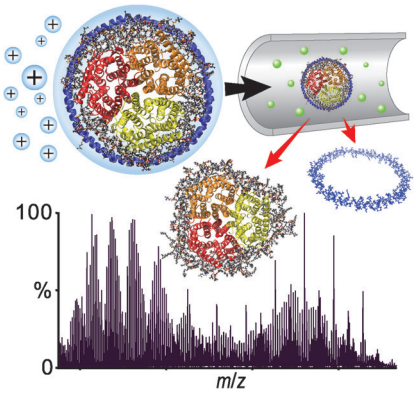

Mass Spectrometry

M. T. Marty, K. K. Hoi, J. Gault, C. V. Robinson* ——— 550 – 554

Probing the Lipid Annular Belt by Gas-Phase Dissociation of Membrane Proteins in Nanodiscs

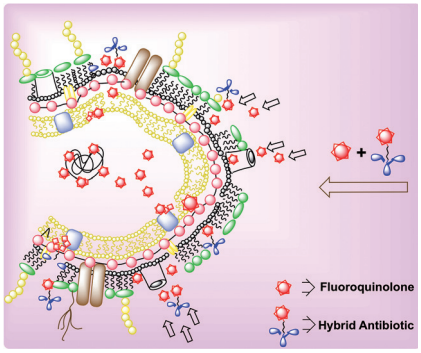

Rescue me: Adjuvants that rescue the activity of fluoroquinolone antibiotics against multidrug-resistant and extremely drug-resistant *Pseudomonas aeruginosa* can be generated by linking tobramycin to ciprofloxacin. The adjuvant combines the antibacterial modes of ciprofloxacin with the membrane-destabilizing effects of aminoglycosides, thereby resulting in enhanced cell penetration of fluoroquinolones and other antibiotics into *P. aeruginosa*.

Antimicrobial Resistance

B. K. Gorityala, G. Guchhait, D. M. Fernando, S. Deo, S. A. McKenna, G. G. Zhanel, A. Kumar, F. Schweizer* ——— 555 – 559

Adjuvants Based on Hybrid Antibiotics Overcome Resistance in *Pseudomonas aeruginosa* and Enhance Fluoroquinolone Efficacy

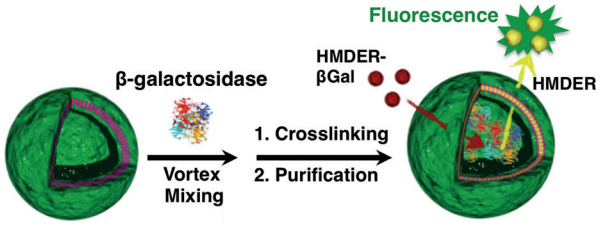

Fragile cargo: By vortex mixing, polyion complex vesicles (PICsomes) were readily loaded with enzymes, which were then delivered to tumor tissue without loss of enzyme activity. Importantly for future therapeutic applications as well as tumor imaging, the enzyme-loaded PICsomes could be used to convert a model prodrug into a highly fluorescent product at the tumor site (see picture).

Nanobiotechnology

Y. Anraku, A. Kishimura,* M. Kamiya, S. Tanaka, T. Nomoto, K. Toh, Y. Matsumoto, S. Fukushima, D. Sueyoshi, M. R. Kano, Y. Urano, N. Nishiyama, K. Kataoka* ——— 560 – 565

Systemically Injectable Enzyme-Loaded Polyion Complex Vesicles as In Vivo Nanoreactors Functioning in Tumors

An organic acid catalyzed direct arylation of aromatic C(sp^2)–H bonds in phenols and naphthols was developed. This transformation is operationally simple, does not require an external oxidant, is readily scaled up, and the structurally diverse biaryls are formed with complete regioselectivity. Density functional calculations suggest a mechanism involving a mixed-acetal formation/[3,3]-sigmatropic rearrangement sequence.

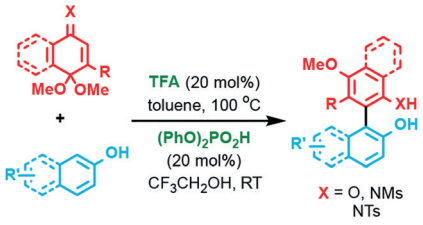

Biaryl Synthesis

H. Gao, Q.-L. Xu, C. Keene, M. Yousufuddin, D. H. Ess, L. Kürti* ——— 566 – 571

Practical Organocatalytic Synthesis of Functionalized Non-C_2-Symmetrical Atropisomeric Biaryls

Drug Delivery

B. Oller-Salvia, M. Sánchez-Navarro, S. Ciudad, M. Guiu, P. Arranz-Gibert, C. Garcia, R. R. Gomis, R. Cecchelli, J. García, E. Giralt,* M. Teixidó* ____ 572 – 575

MiniAp-4: A Venom-Inspired Peptidomimetic for Brain Delivery

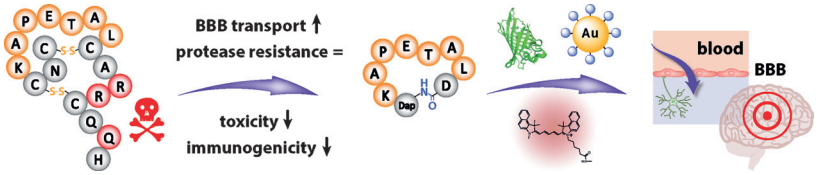

A protease-resistant cyclic peptidomimetic for brain delivery was developed by minimizing the neurotoxin apamin. Toxicity, immunogenicity, and synthetic complexity were decreased while preserving metabolic stability and enhancing transport across the blood–brain barrier (BBB). The new vector is capable of delivering cargoes into the brain parenchyma of mice and across a tight monolayer of human endothelial cells mimicking the BBB.

Inside Cover

Photochromic Proteins

D. Morozov, G. Groenhof* ____ 576 – 578

Hydrogen Bond Fluctuations Control Photochromism in a Reversibly Photo-Switchable Fluorescent Protein

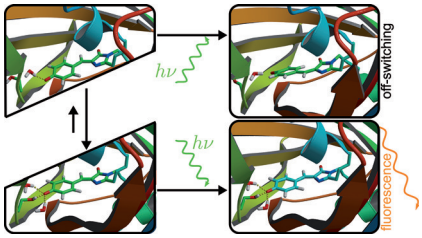

What's going on in Dronpa? Computational simulations reveal that structural heterogeneity divides the ground state ensemble of reversibly photo-switchable fluorescent proteins into two populations, of which the major one fluoresces upon photon absorption, whereas the minor population deactivates into a dark non-fluorescent state.

Aptamers

R. Ueki, A. Ueki, N. Kanda, S. Sando* ____ 579 – 582

Oligonucleotide-Based Mimetics of Hepatocyte Growth Factor

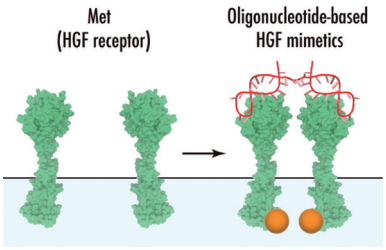

Bridging the gap: A 100-mer ssDNA was developed as a potent hepatocyte growth factor (HGF) mimetic. This ssDNA was designed to induce receptor dimerization at the cell surface and subsequent signal transduction in the same way as the natural growth factor. This new class of synthetic ligands reproduced growth factor induced cellular behaviors, including cell migration and proliferation.

Optical Voltage Sensors

A. Yin, Q. He, Z. Lin, L. Luo, Y. Liu, S. Yang, H. Wu, M. Ding, Y. Huang, X. Duan* ____ 583 – 587

Plasmonic/Nonlinear Optical Material Core/Shell Nanorods as Nanoscale Plasmon Modulators and Optical Voltage Sensors

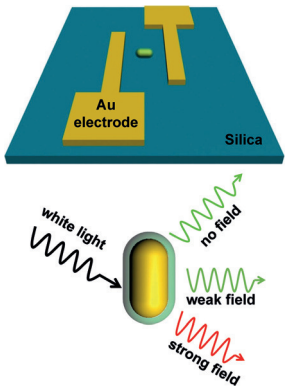

Nanoscale optical voltage sensors: The nanoscale integration of plasmonic and nonlinear optical materials can enable the creation of a new generation of sub-wavelength "electric-plasmonic-optical" modulators and nanoscale optical voltage sensors.

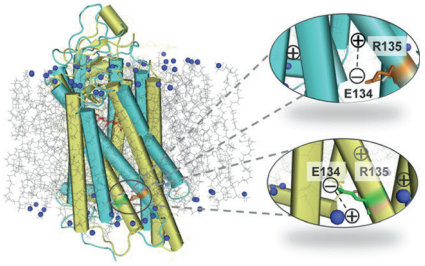

Rhodopsin was incorporated into artificial membranes. The activated MII state (3PXO; yellow) of the membrane-embedded rhodopsin (left) overlaid its dark state (1U19; blue). The cytoplasmic "ionic lock" (i.e. Glu134-Arg135 salt bridge) in the dark state (top right) is broken by attractive charge interactions between the cationic membrane surface moieties and deprotonated Glu134 (bottom right).

Biophysics

U. Chawla, Y. Jiang, W. Zheng, L. Kuang, S. M. D. C. Perera, M. C. Pitman, M. F. Brown,* H. Liang* ____ **588 – 592**

A Usual G-Protein-Coupled Receptor in Unusual Membranes

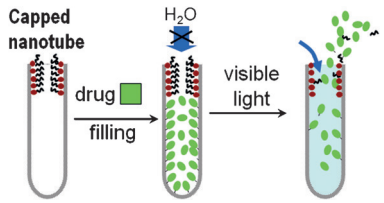

A visible-light-triggered drug delivery system is constructed based on a double-layered stack of TiO_2 nanotubes. The key for visible light drug release is a hydrophobic cap on the nanotubes containing Au nanoparticles, where SPR with the TiO_2 conduction band provides the active species for chain scission. The system was tested in antibacterial experiments against *E. coli*.

Drug Delivery Nanotubes

J. Xu, X. Zhou, Z. Gao, Y.-Y. Song,* P. Schmuki* ____ **593 – 597**

Visible-Light-Triggered Drug Release from TiO_2 Nanotube Arrays: A Controllable Antibacterial Platform

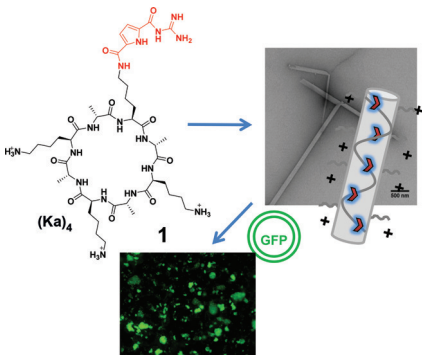

Delivering the goods: After functionalization of the cyclic peptide $(Ka)_4$ with a single guanidiniocarbonyl pyrrole (GCP) moiety, cationic nanofibers of micrometer length are formed. These aggregates are efficient gene transfection vectors. DNA binds to their cationic surface and is efficiently delivered into cells. GFP = green fluorescent protein.

Gene Transfection

M. Li, M. Ehlers, S. Schlesiger, E. Zellermann, S. K. Knauer, C. Schmuck* ____ **598 – 601**

Incorporation of a Non-Natural Arginine Analogue into a Cyclic Peptide Leads to Formation of Positively Charged Nanofibers Capable of Gene Transfection

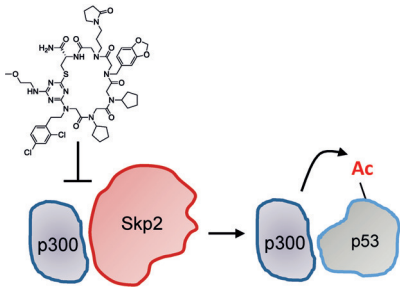

Skp2 inhibitor: The discovery of a chemical inhibitor of the Skp2/p300 interaction is reported. The inhibitor is able to specifically inhibit non-proteolytic activity without affecting Skp2 proteolytic activity. Thus, the inhibitor can be developed as a chemical probe of Skp2 non-proteolytic function during tumorigenesis.

Protein–Protein Interactions

M. Oh, J. H. Lee, H. Moon, Y.-J. Hyun, H.-S. Lim* ____ **602 – 606**

A Chemical Inhibitor of the Skp2/p300 Interaction that Promotes p53-Mediated Apoptosis

Metal–Graphene Catalysis

A. Primo, I. Esteve-Adell, S. N. Coman, N. Candu, V. I. Parvulescu,* H. Garcia* ——— 607 – 612

One-Step Pyrolysis Preparation of 1.1.1 Oriented Gold Nanoplatelets Supported on Graphene and Six Orders of Magnitude Enhancement of the Resulting Catalytic Activity

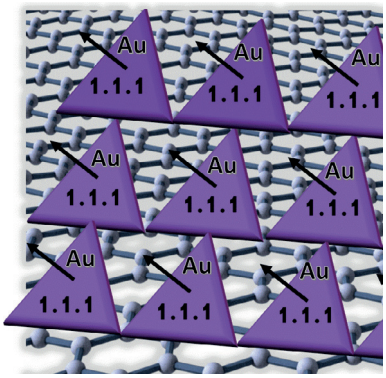

Easy gold–graphene nanohybrid catalysts: Graphene and 1.1.1 facet-oriented Au nanoparticles form simultaneously upon pyrolysis of chitosan-embedding $AuCl_4^-$, and exhibit high catalytic activity.

P_4 Functionalization

J. E. Borger, A. W. Ehlers, M. Lutz, J. C. Slootweg, K. Lammertsma* ——— 613 – 617

Stabilization and Transfer of the Transient $[Mes^*P_4]^-$ Butterfly Anion Using BPh_3

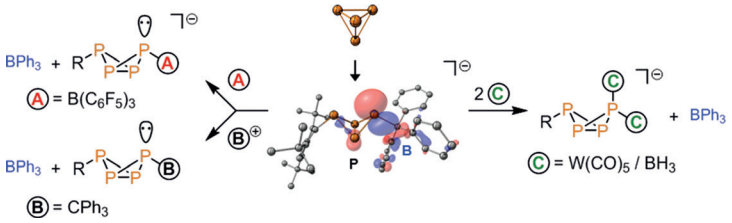

Trap and transfer: The bicyclo-[1.1.0]tetraphosphabutane anion (see scheme, center), generated from P_4 and Mes*Li (Mes* = 2,4,6-$tBu_3C_6H_2$), can be trapped by BPh_3 in THF. The anion can be used as an $[RP_4]^-$ transfer agent, reacting with neutral Lewis acids ($B(C_6F_5)_3$, BH_3, and $W(CO)_5$) to afford unique singly and doubly coordinated butterfly anions and with the trityl cation to form a neutral, nonsymmetrical P_4 derivative.

Protein Folding

J. Adamcik, A. Sánchez-Ferrer, N. Ait-Bouziad, N. P. Reynolds, H. A. Lashuel,* R. Mezzenga* 618 – 622

Microtubule-Binding R3 Fragment from Tau Self-Assembles into Giant Multistranded Amyloid Ribbons

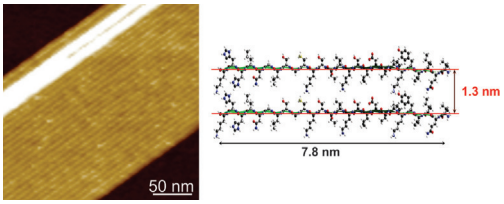

Record-breaking amyloid sheets: The self-assembly of microtubule-binding R3 fragment from Tau protein in the absence of heparin induces the formation of record-length, well-ordered, 2D laminated amyloid ribbon structures.

Surface Chemistry

F. Xiong, Y.-Y. Yu, Z. Wu, G. Sun, L. Ding, Y. Jin, X.-Q. Gong,* W. Huang* 623 – 628

Methanol Conversion into Dimethyl Ether on the Anatase TiO_2(001) Surface

Let's face't: The methanol-to-dimethyl ether (DME) reaction was unambiguously identified to occur by the dehydration coupling of methoxy species at the four-fold-coordinated Ti^{4+} sites (Ti_{4c}) on a mineral anatase TiO_2(001)-(1×4) surface. The results show, for the first time, the predicted higher reactivity of this facet relative to other reported TiO_2 facets.

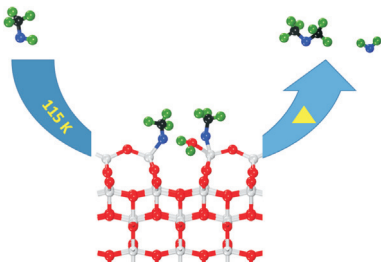

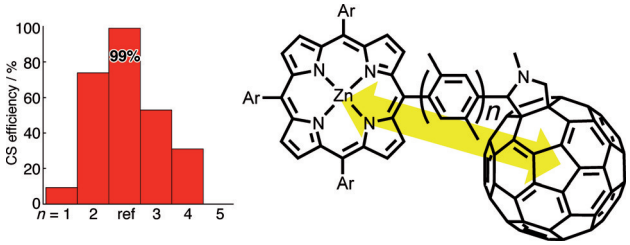

Optimization of donor–acceptor electronic coupling remarkably inhibits the undesirable rapid decay of the singlet charge-separated state to the ground state, yielding the final long-lived, triplet charge-separated state with circa 100% efficiency. This finding is relevant to the rational design of artificial photosynthesis and organic photovoltaic cells.

Charge Separation

T. Higashino, T. Yamada, M. Yamamoto, A. Furube, N. V. Tkachenko,* T. Miura, Y. Kobori,* R. Jono, K. Yamashita,* H. Imahori* _____ **629 – 633**

Remarkable Dependence of the Final Charge Separation Efficiency on the Donor–Acceptor Interaction in Photoinduced Electron Transfer

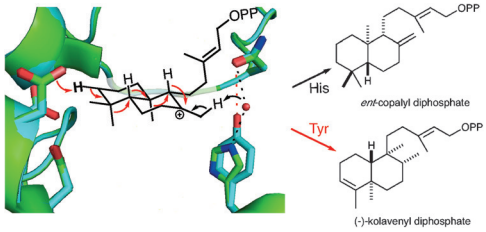

Make the swap: Substitution of histidine, comprising part of the catalytic base group in the *ent*-copalyl diphosphate synthases, leads to rearrangements. Through a series of 1,2-hydride and methyl shifts of the initially formed bicycle, predominant formation of (−)-kolavenyl diphosphate is observed. Further mutational analysis and quantum chemical calculations provide mechanistic insight into the basis for this profound effect on product outcome.

Enzyme Catalysis

K. C. Potter, J. Zi, Y. J. Hong, S. Schulte, B. Malchow, D. J. Tantillo, R. J. Peters* _____ **634 – 638**

Blocking Deprotonation with Retention of Aromaticity in a Plant *ent*-Copalyl Diphosphate Synthase Leads to Product Rearrangement

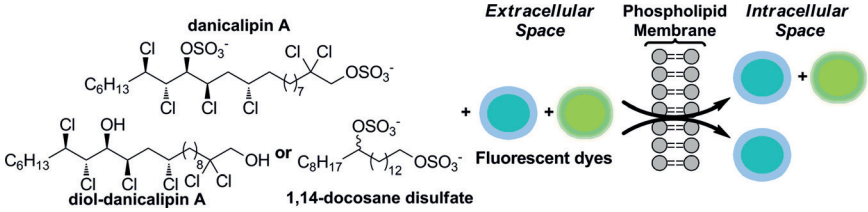

Enhanced membrane permeability: The effects of the chlorosulfolipid danicalipin A on the membranes of mammalian cells and on the walls of Gram-negative bacteria are investigated. These studies were enabled through the development of a novel, scalable synthesis. The ability of danicalipin A to facilitate the diffusion of fluorescent dyes into cells is described.

Chlorosulfolipids

A. M. Bailey, S. Wolfrum, E. M. Carreira* _____ **639 – 643**

Biological Investigations of (+)-Danicalipin A Enabled Through Synthesis

Lithium carbide (Li_2C_2) is shown to function as a potential cathode material for lithium ion batteries. At least half of the lithium can be extracted and reinserted in Li_2C_2 during cycling. These results open the door to future applications of alkali and alkaline earth metal electrodes.

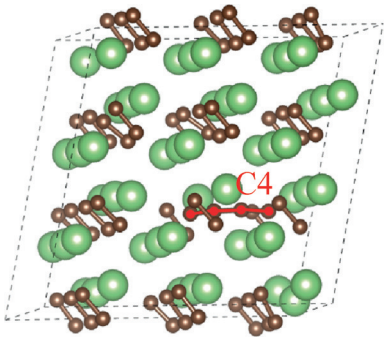

Lithium Ion Batteries

N. Tian, Y. Gao, Y. Li, Z. Wang,* X. Song, L. Chen _____ **644 – 648**

Li_2C_2, a High-Capacity Cathode Material for Lithium Ion Batteries

1,2,3-Triazoles

W. Wang, X. Peng, F. Wei, C.-H. Tung, Z. Xu* ——— 649 – 653

Copper(I)-Catalyzed Interrupted Click Reaction: Synthesis of Diverse 5-Hetero-Functionalized Triazoles

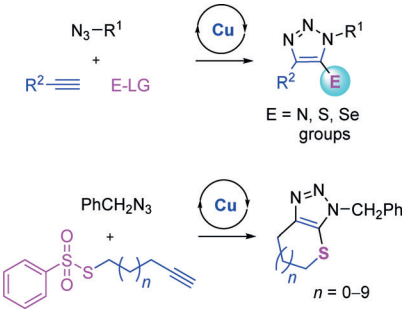

A copper(I)-catalyzed interrupted click reaction to access diverse 5-functionalized triazoles is reported. Various 5-amino-, 5-thio-, and 5-selenotriazoles were assembled in a single step in high yields. The reaction proceeds under mild conditions with complete regioselectivity and features a broad substrate scope and compatibility with various functional groups.

Structural Biology

C. De Castro,* I. Speciale, G. Duncan, D. D. Dunigan, I. Agarkova, R. Lanzetta, L. Sturiale, A. Palmigiano, D. Garozzo, A. Molinaro, M. Tonetti, J. L. Van Etten ——— 654 – 658

N-Linked Glycans of Chloroviruses Sharing a Core Architecture without Precedent

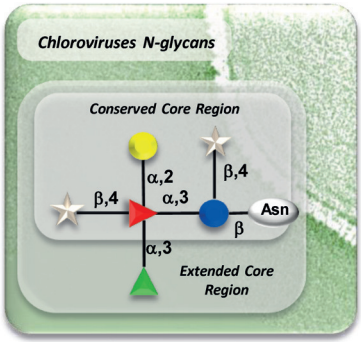

Glycan signature: Chloroviruses glycosylate their capsid protein in a host-independent process. These N-linked glycans have unprecedented structures, and each is virus-specific, but all share the same core motif. Conservation in the core region occurs at two different levels: the most conserved region comprises five residues and inclusion of the sixth extends this strictly conserved core. This core oligosaccharide represents a new type of N-glycosylation.

Self-Assembly

N. Bilbao, I. Destoop, S. De Feyter,* D. González-Rodríguez* ——— 659 – 663

Two-Dimensional Nanoporous Networks Formed by Liquid-to-Solid Transfer of Hydrogen-Bonded Macrocycles Built from DNA Bases

DNA base pairing is used to produce hydrogen-bonded macrocycles whose supramolecular structure can be transferred from solution to a solid substrate. A hierarchical assembly process ultimately leads to two-dimensional nanostructured porous networks that are able to host size-complementary guests.

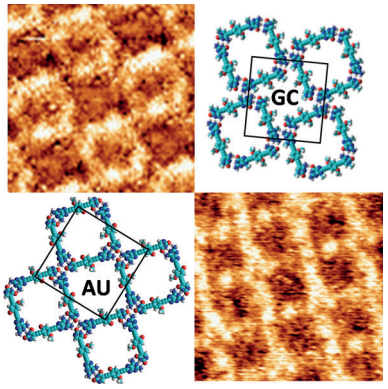

Biosynthesis

R. V. K. Cochrane, R. Sanichar, G. R. Lambkin, B. Reiz, W. Xu, Y. Tang, J. C. Vederas* ——— 664 – 668

Production of New Cladosporin Analogues by Reconstitution of the Polyketide Synthases Responsible for the Biosynthesis of this Antimalarial Agent

The highly reducing and non-reducing polyketide synthase pair that is responsible for the production of cladosporin in *Cladosporium cladosporioides* has been identified and heterologously expressed, and its functional activity has been demonstrated. A putative lysyl-tRNA synthetase is also contained within the cladosporin gene cluster and proposed to be necessary for self-resistance in the organism.

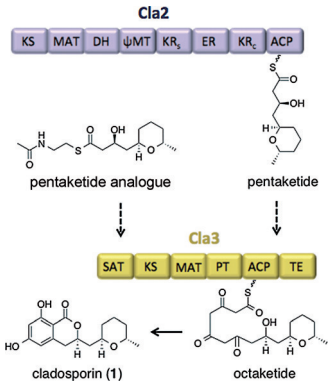

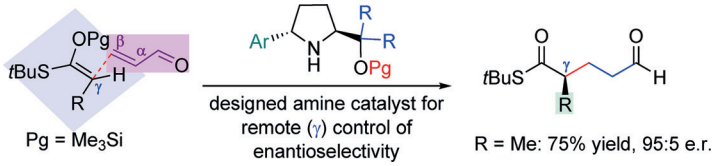

Organocatalysis

A. Claraz, G. Sahoo, D. Berta, Á. Madarász, I. Pápai, P. M. Pihko* ——— **669 – 673**

A Catalyst Designed for the Enantioselective Construction of Methyl- and Alkyl-Substituted Tertiary Stereocenters

Methyls by design: Systematic three-point optimization affords an amine catalyst which provides ready access to chiral α-methyl-substituted and other α-alkyl-substituted thioesters in high enantiomeric purity (see example). Natural product building blocks, such as the C4–C13 segment of bistramide A, can be quickly accessed with the catalyst.

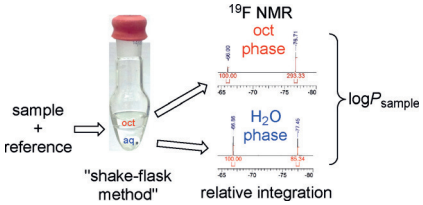

Lipophilicity

B. Linclau,* Z. Wang, G. Compain, V. Paumelle, C. Q. Fontenelle, N. Wells, A. Weymouth-Wilson ——— **674 – 678**

Investigating the Influence of (Deoxy)fluorination on the Lipophilicity of Non-UV-Active Fluorinated Alkanols and Carbohydrates by a New log *P* Determination Method

A variation of the "shake-flask method" was developed for the straightforward determination of the lipophilicity (log *P*) of fluorinated compounds and is based on the relative integration of the ^{19}F NMR peaks of a sample and an internal reference for each phase (oct = octanol). The influence of different fluorination motifs on the lipophilicity of various aliphatic alkanols and carbohydrates was determined.

Stacking blocks: Two nanosized $Mn_{25}Na_4$ and Mn_{49} clusters consisting of four and eight decametallic supertetrahedral subunits, respectively, are reported. These clusters are unique examples of oligomeric species based on magnetic subunits and have large spin ground-state values $S = 51/2$ ($Mn_{25}Na_4$) and 61/2 (Mn_{49}). The Mn_{49} cluster displays single-molecule magnet (SMM) behavior and is the second largest reported homometallic SMM.

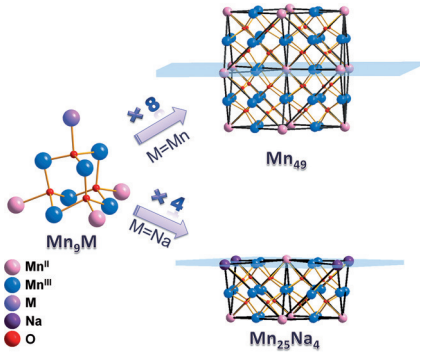

Cluster Compounds

M. Manoli, S. Alexandrou, L. Pham, G. Lorusso, W. Wernsdorfer, M. Evangelisti, G. Christou, A. J. Tasiopoulos* ——— **679 – 684**

Magnetic "Molecular Oligomers" Based on Decametallic Supertetrahedra: A Giant Mn_{49} Cuboctahedron and its $Mn_{25}Na_4$ Fragment

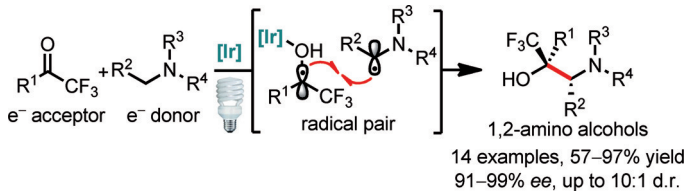

Photoredox Catalysis

C. Wang, J. Qin, X. Shen, R. Riedel, K. Harms, E. Meggers* ——— **685 – 688**

Asymmetric Radical–Radical Cross-Coupling through Visible-Light-Activated Iridium Catalysis

Combining single electron transfer between a donor substrate and a catalyst-activated acceptor substrate with a stereocontrolled radical–radical recombination enables the visible-light-driven synthesis of 1,2-amino alcohols from trifluoromethyl ketones and tertiary amines. With a chiral iridium complex acting as both a Lewis acid and a photoredox catalyst, enantioselectivities of up to 99% *ee* were achieved.

Peptide Structure

V. Kopysov, O. V. Boyarkin* — 689 – 692

Resonance Energy Transfer Relates the Gas-Phase Structure and Pharmacological Activity of Opioid Peptides

Inside Back Cover

The FRET of pain: Resonance energy transfer, detected by a combination of cold ion spectroscopy and mass spectrometry, is used to estimate the Tyr–Phe spacing for enkephalins in the gas phase. These distances appear to differ substantially in enkephalins (pain-relief drugs) with different pharmacological efficiencies.

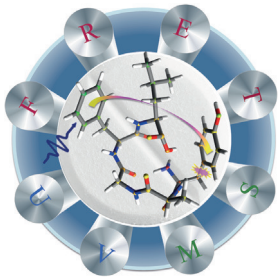

Electrocatalysis

Y. Kuang, G. Feng, P. Li, Y. Bi, Y. Li, X. Sun* — 693 – 697

Single-Crystalline Ultrathin Nickel Nanosheets Array from In Situ Topotactic Reduction for Active and Stable Electrocatalysis

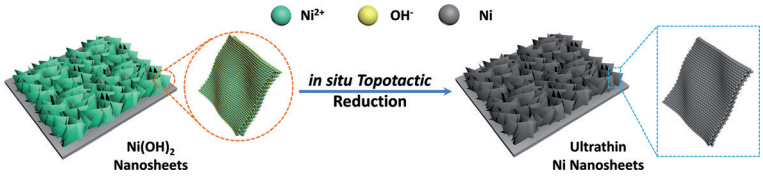

Low-cost electrocatalysts: Ultrathin nickel nanosheets were synthesized by gently reducing a $Ni(OH)_2$ nanosheet array on a metal substrate (see picture). The electrocatalytic performance of the Ni nanosheets was tested on the oxidation of hydrazine and the hydrogen-evolution reaction.

CO_2 Reduction

S. Gao, X. Jiao, Z. Sun, W. Zhang, Y. Sun,* C. Wang, Q. Hu, X. Zu, F. Yang, S. Yang, L. Liang, J. Wu, Y. Xie* — 698 – 702

Ultrathin Co_3O_4 Layers Realizing Optimized CO_2 Electroreduction to Formate

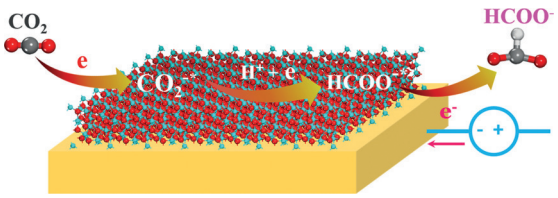

The thinner, the better: 1.72 nm thick Co_3O_4 layers were synthesized through a fast-heating strategy. Benefiting from the ultralarge fraction of surface atoms and increased density of states, the 1.72 nm thick Co_3O_4 layers are active in the electrocatalytic reduction of CO_2 to formate and have a current density over 20 times higher than bulk samples.

Molecular Machines

A. Goujon, G. Du, E. Moulin, G. Fuks, M. Maaloum, E. Buhler, N. Giuseppone* — 703 – 707

Hierarchical Self-Assembly of Supramolecular Muscle-Like Fibers

Supramolecular polymers: The integrated actuation of switchable mechanical bonds in bundles of supramolecular polymers leads to dynamic mesostructures (see picture). A new kind of hydrogen-bonded supramolecular polymers is described which incorporate molecular machines in the form of acid–base switchable [*c*2]daisy chain rotaxanes.

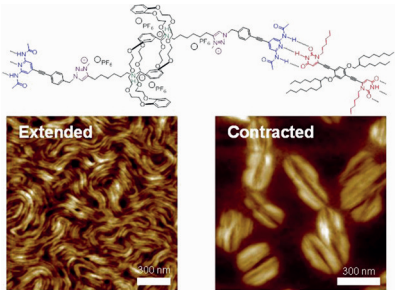

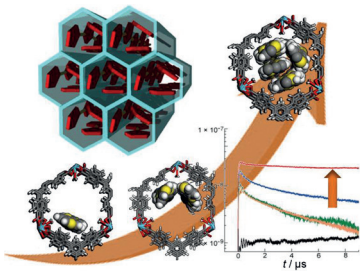

Solitary confinement: The controlled assembly of polythiophene within the channels of a metal–organic framework was carried out. This system was used to demonstrate the assembly packing structure as a way of controlling the optical and electronic properties of the conjugated polymer.

Metal–Organic Frameworks

M. W. A. MacLean, T. Kitao, T. Suga, M. Mizuno, S. Seki, T. Uemura,* S. Kitagawa* ——— **708 – 713**

Unraveling Inter- and Intrachain Electronics in Polythiophene Assemblies Mediated by Coordination Nanospaces

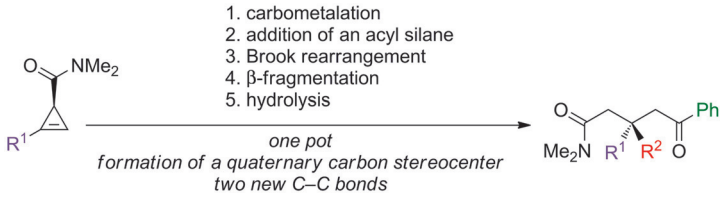

How many steps? One great stride: The regio- and stereoselective carbometalation of cyclopropenyl amides and addition of an acyl silane gave polysubstituted cyclopropyl derivatives, which underwent a Brook rearrangement with inversion of configuration and selective ring cleavage when the reaction mixture was warmed to room temperature. Hydrolysis then completed the one-pot synthesis of δ-keto-amides with a quaternary stereocenter (see scheme).

Synthetic Methods

F.-G. Zhang, G. Eppe, I. Marek* ——— **714 – 718**

Brook Rearrangement as a Trigger for the Ring Opening of Strained Carbocycles

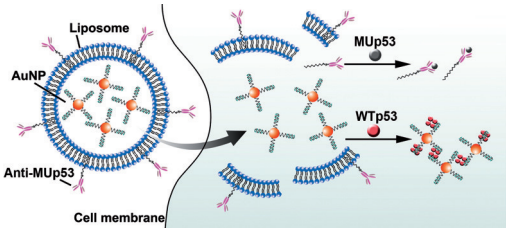

Wild and mutant imaging: Dual-targeting nanovesicles based on consensus DNA-functionalized plasmonic gold nanoparticles (AuNPs) are designed and used for the simultaneous plasmonic imaging of wild-type p53 and fluorescence imaging of mutant p53.

Intracellular Targeting

R. Qian, Y. Cao, Y.-T. Long* ——— **719 – 723**

Dual-Targeting Nanovesicles for In Situ Intracellular Imaging of and Discrimination between Wild-type and Mutant p53

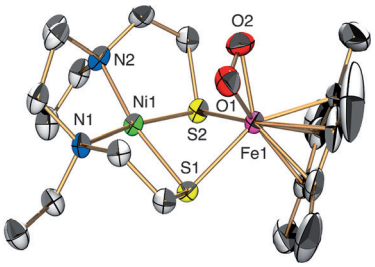

Dioxygen-tolerant [NiFe] hydrogenases catalyze not only the conversion of H_2 into $2H^+$ and $2e^-$ but also the reduction of O_2 to H_2O. A new [NiFe]-based complex is a synthetic mimic of such hydrogenases and catalyzes O_2 reduction via an O_2 adduct, which was shown to be the first example of a side-on iron(IV) peroxo complex.

Hydrogenases

T. Kishima, T. Matsumoto, H. Nakai, S. Hayami, T. Ohta, S. Ogo* ——— **724 – 727**

A High-Valent Iron(IV) Peroxo Core Derived from O_2

Back Cover

Membrane Proteins

A. J. Y. Jones, J. N. Blaza, H. R. Bridges, B. May, A. L. Moore, J. Hirst* ... 728 – 731

A Self-Assembled Respiratory Chain that Catalyzes NADH Oxidation by Ubiquinone-10 Cycling between Complex I and the Alternative Oxidase

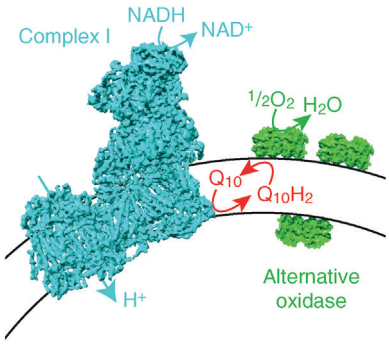

Chained together: Mitochondrial complex I is crucial for respiration, but its reactions with ubiquinone-10 (Q_{10}) are poorly understood because Q_{10} is extremely hydrophobic. An artificial electron transport chain comprising complex I, Q_{10}, and a quinol oxidase was self-assembled in synthetic vesicles and used to study Q_{10} reduction in a fully defined environment. This self-assembled system is suitable for studying any enzyme that uses a quinone/quinol substrate.

Analytical Chemistry

J. J. Zhang, Y. Xiang, M. Wang, A. Basu, Y. Lu* ... 732 – 736

Dose-Dependent Response of Personal Glucose Meters to Nicotinamide Coenzymes: Applications to Point-of-Care Diagnostics of Many Non-Glucose Targets in a Single Step

Glucose & Personal: A wide range of non-glucose targets can be detected by using the dose-dependent response of personal glucose meters to nicotinamide coenzymes, such as the reduced form of nicotinamide adenine dinucleotide (NADH). Cascade enzymatic reactions result in the target-induced consumption or production of NADH, which in turn is detected by the glucose meter. This point-of-care device can be used for highly sensitive blood analysis in a single step.

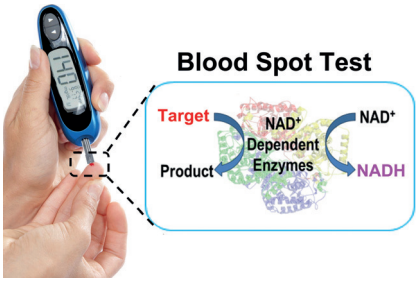

Heterogeneous Catalysis

Z. He, Q. Qian, J. Ma, Q. Meng, H. Zhou, J. Song, Z. Liu, B. Han* ... 737 – 741

Water-Enhanced Synthesis of Higher Alcohols from CO_2 Hydrogenation over a Pt/Co_3O_4 Catalyst under Milder Conditions

Water can enhance the synthesis of C_2–C_4 alcohols ($C_{2+}OH$) from CO_2 hydrogenation over Pt/Co_3O_4 significantly. The alcohols can be produced at a lower temperature with satisfactory activity and selectivity. DMI = 1,3-dimethyl-2-imidazolidinone.

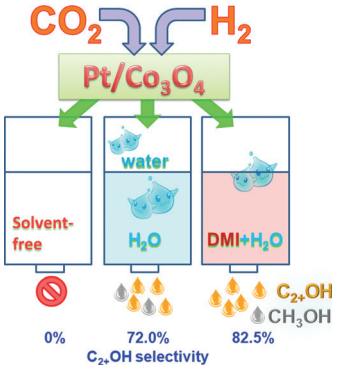

Hydrogen Production Catalysts

P. Lettenmeier, L. Wang, U. Golla-Schindler, P. Gazdzicki, N. A. Cañas, M. Handl, R. Hiesgen, S. S. Hosseiny, A. S. Gago,* K. A. Friedrich ... 742 – 746

Nanosized IrO_x–Ir Catalyst with Relevant Activity for Anodes of Proton Exchange Membrane Electrolysis Produced by a Cost-Effective Procedure

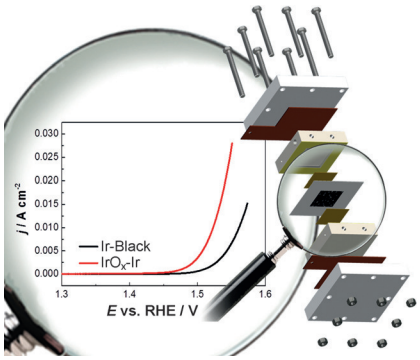

Electrolysis: The environmentally friendly synthesis of a highly active iridium-based oxygen evolution reaction (OER) catalyst for proton exchange membrane (PEM) electrolysis is reported. The catalyst is capable of significantly decreasing the reaction overpotential, allowing for more sustainable hydrogen production.

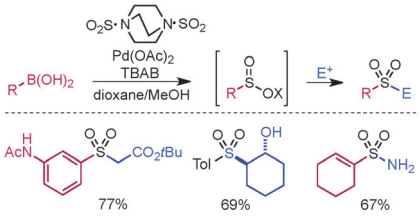

Staying neutral: $Pd(OAc)_2$ promotes the addition of aryl and heteroaryl boronic acids to the sulfur dioxide surrogate 1,4-diazabicyclo[2.2.2]octane bis(sulfur dioxide) (DABSO) thus delivering the corresponding sulfinates. When combined with an electrophilic trap, this redox-neutral system provides a straightforward route for the one-pot preparation of a broad range of sulfones and sulfonamides.

Synthetic Methods

A. S. Deeming, C. J. Russell, M. C. Willis* ——— 747 – 750

Palladium(II)-Catalyzed Synthesis of Sulfinates from Boronic Acids and DABSO: A Redox-Neutral, Phosphine-Free Transformation

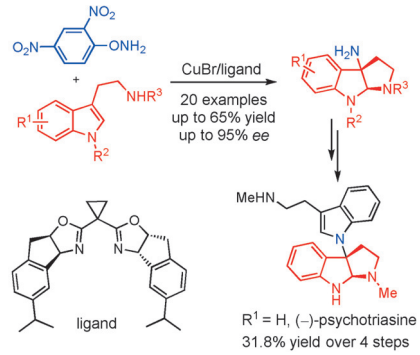

A direct asymmetric dearomative amination of tryptamines with O-(2,4-dinitrophenyl)hydroxylamine (DPH) was achieved using CuBr-bisoxazoline complex as a catalyst, affording 3a-amino-pyrroloindolines in good enantioselectivity under mild reaction conditions. The synthetic value of this method was demonstrated in the total synthesis of (−)-psychotriasine in a highly concise manner.

Synthetic Methods

C. Liu, J.-C. Yi, Z.-B. Zheng, Y. Tang,* L.-X. Dai, S.-L. You* ——— 751 – 754

Enantioselective Synthesis of 3a-Amino-Pyrroloindolines by Copper-Catalyzed Direct Asymmetric Dearomative Amination of Tryptamines

Reliable transport and delivery: Bioreducible cationic nanomicelles exhibited remarkably high DNA-binding affinity to completely condense DNA at an N/P ratio of 1. The efficiency with which the resulting nanomicelle/DNA polyplexes delivered genes into cells was much higher than that of a cationic polymer (see picture). In some cases, even at a low N/P ratio of 2, the gene-transfection efficiency was similar to that observed with viral vectors.

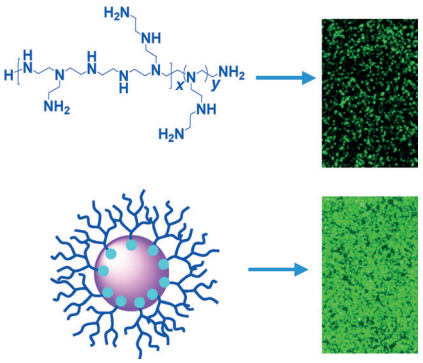

Gene Delivery

L. Wang, D. Wu, H. Xu, Y. You* ——— 755 – 759

High DNA-Binding Affinity and Gene-Transfection Efficacy of Bioreducible Cationic Nanomicelles with a Fluorinated Core

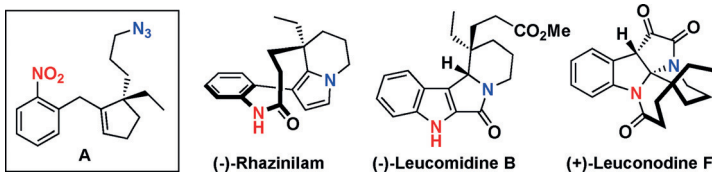

Be divergent: Concise total syntheses of (−)-rhazinilam, (−)-leucomidine B, and (+)-leuconodine F were accomplished from the common intermediate **A**. A homogeneous palladium catalyst was exploited for the first time to accomplish a substrate-directed highly diastereoselective hydrogenation of a sterically unbiased double bond. A self-induced diastereomeric anisochronism (SIDA) phenomenon was observed for leucomidine B.

Natural Product Synthesis

D. Dagoneau, Z. Xu, Q. Wang, J. Zhu* ——— 760 – 763

Enantioselective Total Syntheses of (−)-Rhazinilam, (−)-Leucomidine B, and (+)-Leuconodine F

Photochemistry

R. L. Sutar, E. Levin, D. Butilkov, I. Goldberg, O. Reany, N. G. Lemcoff* ——— 764 – 767

A Light-Activated Olefin Metathesis Catalyst Equipped with a Chromatic Orthogonal Self-Destruct Function

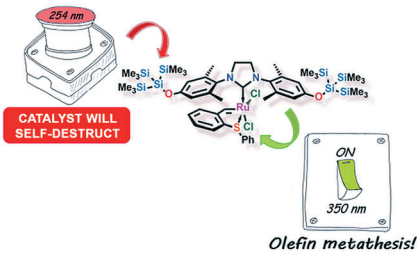

Light giveth and light taketh: A new catalyst promotes olefin metathesis when irradiated with UV-A and is decomposed by UV-C. Complex light-guided chemical processes based on olefin metathesis, including polymerization, can be carried out by this protocol.

Micelles

S. Uchiyama,* E. Fukatsu, G. D. McClean, A. P. de Silva* ——— 768 – 771

Measurement of Local Sodium Ion Levels near Micelle Surfaces with Fluorescent Photoinduced-Electron-Transfer Sensors

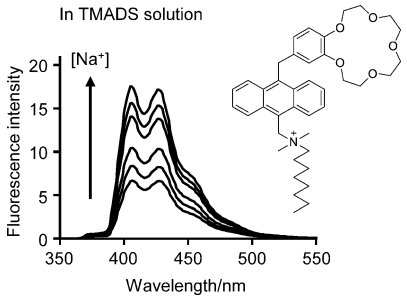

The local Na^+ concentration near an anionic tetramethylammonium dodecyl sulfate (TMADS) micelle surface was determined with new fluorescent photo-induced electron transfer (PET) sensors. Electrostatic interactions with the negatively charged sulfonate groups of the surfactant induce an increase in the Na^+ concentration compared with bulk water.

Energetic Materials

C. He, J. M. Shreeve* ——— 772 – 775

Potassium 4,5-Bis(dinitromethyl)-furoxanate: A Green Primary Explosive with a Positive Oxygen Balance

Green primers: Potassium 4,5-bis(dinitromethyl)furoxanate (see structure) was prepared by the nitration of 4,5-dichloroximefuroxan, followed by treatment with potassium iodide. Its high sensitivity and detonation performance along with its positive oxygen balance endow it with high potential as a green primary explosive for the replacement of lead azide.

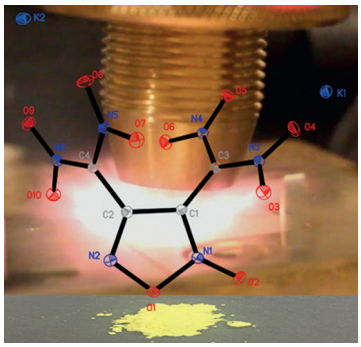

Alkene Hydroamination

Y. Xi, T. W. Butcher, J. Zhang, J. F. Hartwig* ——— 776 – 780

Regioselective, Asymmetric Formal Hydroamination of Unactivated Internal Alkenes

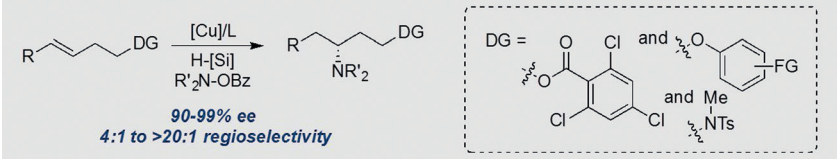

A regio- and enantioselective formal hydroamination of unsymmetrical, unactivated internal alkenes occurs with a silane and hydroxylamine derivative. The regioselectivity is controlled by the electronic effects of ether, ester, and sulfonamide groups in the homoallylic position. This method provides direct access to 1,3-aminoalcohols with high enantioselectivity.

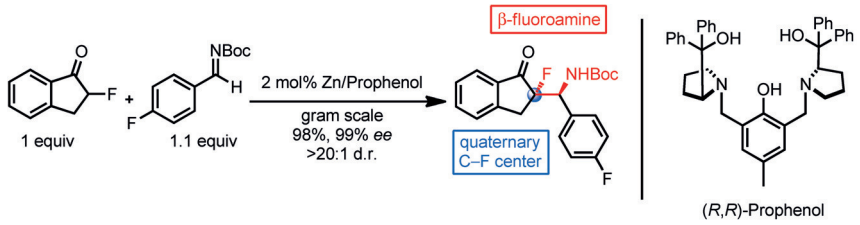

Work of a Pro: A Zn/Prophenol-catalyzed direct Mannich reaction using α-fluoroketones allows efficient construction of β-fluoroamine motifs with high enantio- and diastereoselectivities. A stereocomplementary aldol reaction is also described. Boc = *tert*-butoxycarbonyl.

Asymmetric Catalysis

B. M. Trost,* T. Saget, A. Lerchen, C.-I. Hung ——— **781 – 784**

Catalytic Asymmetric Mannich Reactions with Fluorinated Aromatic Ketones: Efficient Access to Chiral β-Fluoroamines

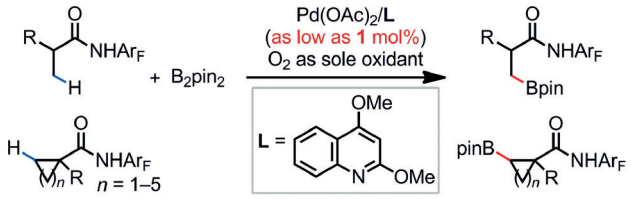

A quinoline-based ligand promotes the efficient palladium-catalyzed borylation of primary β-C(sp³)–H bonds in carboxylic acid derivatives as well as secondary C(sp³)–H bonds in a variety of carbocycles. This directed borylation method complements existing iridium(I)- and rhodium(I)-catalyzed C–H borylation reactions in terms of scope and reaction conditions.

C–H Activation

J. He, H. Jiang, R. Takise, R.-Y. Zhu, G. Chen, H.-X. Dai, T. G. M. Dhar, J. Shi, H. Zhang, P. T. W. Cheng, J.-Q. Yu* ——— **785 – 789**

Ligand-Promoted Borylation of C(sp³)–H Bonds with Palladium(II) Catalysts

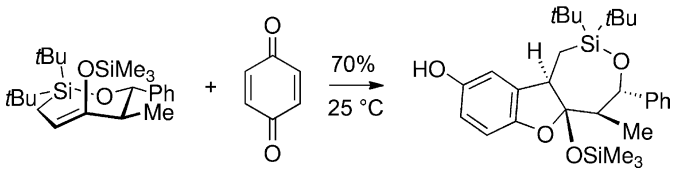

***trans*-Oxasilacycloheptenes** are strained seven-membered-ring *trans*-alkenes that underwent [4+2] cycloaddition reactions faster than a bicyclic *trans*-cyclooctene. They also reacted with quinones and dimethyl acetylenedicarboxylate to form adducts with high diastereoselectivity. Kinetic studies showed that ring strain increases nucleophilicity by approximately 10^9.

Strained Molecules

J. R. Sanzone, K. A. Woerpel* ——— **790 – 793**

High Reactivity of Strained Seven-Membered-Ring *trans*-Alkenes

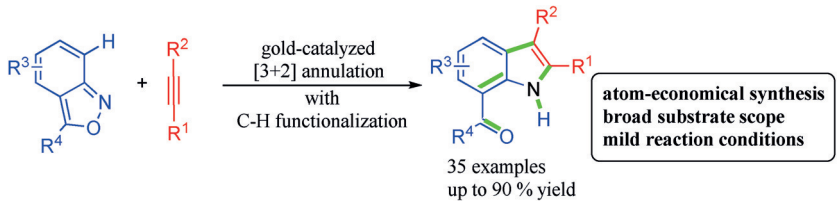

Good as gold: The gold-catalyzed C–H annulation of anthranil derivatives with alkynes offers a facile, flexible, and atom-economical one-step route to unprotected 7-acylindoles. The reaction proceeds via an α-imino gold carbene intermediate, which promotes *ortho*-aryl C–H functionalization to afford the product. The transformation proceeds with a broad range of substrates under mild conditions.

Gold Catalysis

H. Jin, L. Huang, J. Xie, M. Rudolph, F. Rominger, A. S. K. Hashmi* **794 – 797**

Gold-Catalyzed C–H Annulation of Anthranils with Alkynes: A Facile, Flexible, and Atom-Economical Synthesis of Unprotected 7-Acylindoles

Oxygenations

Y. Ni, E. Fernández-Fueyo, A. G. Baraibar, R. Ullrich, M. Hofrichter, H. Yanase, M. Alcalde, W. J. H. van Berkel, F. Hollmann* ——— 798 – 801

Peroxygenase-Catalyzed Oxyfunctionalization Reactions Promoted by the Complete Oxidation of Methanol

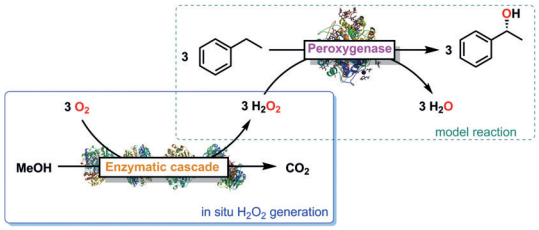

Fueled by methanol: Peroxygenases catalyze stereoselective oxyfunctionalizations by utilizing H_2O_2. To efficiently generate this oxidant in situ, a new enzymatic cascade process for the reductive activation of molecular oxygen with methanol as a stoichiometric reductant has been developed. This system was applied to the stereoselective hydroxylation of ethylbenzene to (*R*)-1-phenylethanol.

Aryne Chemistry

Y. Li, S. Chakrabarty, C. Mück-Lichtenfeld, A. Studer* ——— 802 – 806

Ortho-Trialkylstannyl Arylphosphanes by C–P and C–Sn Bond Formation in Arynes

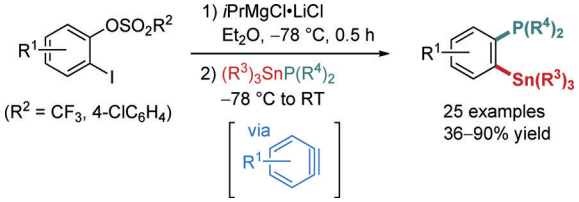

Aryne insertion of stannylated phosphanes ($R_3Sn{-}PR_2$) occurs with high yields under mild conditions. *ortho*-Stannylarylphosphanes obtained in this reaction are highly valuable compounds for follow-up transformations.

Drug Design

A. C. Lai, M. Toure, D. Hellerschmied, J. Salami, S. Jaime-Figueroa, E. Ko, J. Hines, C. M. Crews* ——— 807 – 810

Modular PROTAC Design for the Degradation of Oncogenic BCR-ABL

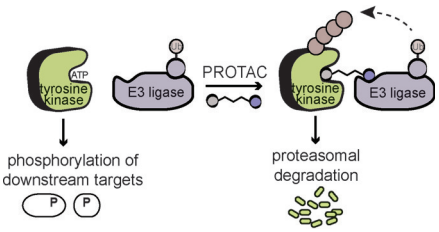

Induced protein degradation is an emerging field that has the potential to overcome many challenges faced by traditional inhibitor-based drug design. A modular approach to PROTAC design is presented that enables targeted degradation of the therapeutically relevant BCR-ABL oncogenic protein.

Molecular Dynamics

T. Stauch, A. Dreuw* ——— 811 – 814

Knots "Choke Off" Polymers upon Stretching

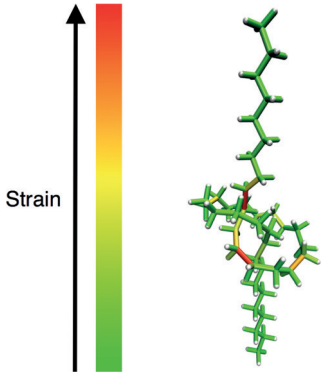

The force chokes: A polymer chain is substantially weakened by a knot and ruptures at its "entry" or "exit", because the torsions in the curved part of the chain act as "work funnels" that localize the mechanical stress in this region. As a result, the knot chokes off the chain in its immediate vicinity. This shows that bonds do not have to be extensively stretched to be broken in mechanochemical pulling experiments.

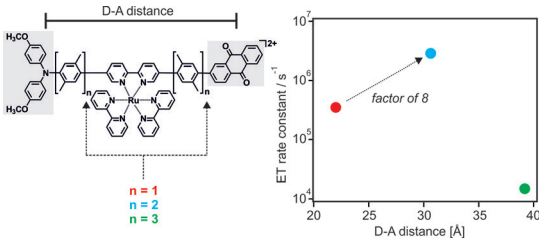

Usually electron-transfer rates decrease with increasing separation between the donor and the acceptor. However, the interplay between reorganization energy and electronic coupling can lead to opposite, counter-intuitive behavior.

Electron Transfer

M. Kuss-Petermann, O. S. Wenger* ——— 815 – 819

Increasing Electron-Transfer Rates with Increasing Donor–Acceptor Distance

Supporting information is available on www.angewandte.org (see article for access details).

A video clip is available as Supporting Information on www.angewandte.org (see article for access details).

This article is available online free of charge (Open Access).

This article is accompanied by a cover picture (front or back cover, and inside or outside).

The Very Important Papers, marked VIP, have been rated unanimously as very important by the referees.

The Hot Papers are articles that the Editors have chosen on the basis of the referee reports to be of particular importance for an intensely studied area of research.

Check out these journals: